Title

Quantifying the Cribriform Plate: Influences of Allometry, Function, and Phylogeny in Carnivora

Journal

The Anatomical Record, 297(11)

ISSN

1932-8486

Authors

Bird, Deborah J
Amirkhanian, Arsineh
Pang, Benison
et al.

Publication Date

2014-11-01

DOI

10.1002/ar.23032

Peer reviewed

THE ANATOMICAL RECORD 297:2080–2092 (2014)

Quantifying the Cribriform Plate: Influences of Allometry, Function, and Phylogeny in Carnivora

DEBORAH J. BIRD,* ARSINEH AMIRKHANIAN, BENISON PANG, AND BLAIRE VAN VALKENBURGH
Department of Ecology and Evolutionary Biology, UCLA, Los Angeles, California

ABSTRACT

The small, perforated bony cup of the anterior cranial fossa called the cribriform plate (CP) is perhaps the best-preserved remnant of olfactory anatomy in fossil mammal skulls. The CP and its myriad foramina record the passage of peripheral olfactory nerves from nasal cavity to olfactory bulb. Previous work has suggested that CP surface area reflects aspects of olfactory capacity (as inferred from habitat and observed behavior) in mammals. To further explore the utility of CP as a proxy for olfactory function, we designed novel, nondestructive digital methods to quantify CP morphology from dry skulls. Using CT scans and 3-D imaging software, we quantified CP features from 42 species of Carnivora, a group that represents a wide spectrum of ecologies and sensory demands. Two metrics, CP surface area (CPSA) and cumulative CP foramina area (FXSA), scaled to skull length with negative allometry, and differed between aquatic and terrestrial species, with the former having reduced areas. Number of foramina (NF) was not correlated with skull length but tended to be greater in caniforms than feliforms. Both CPSA and FXSA are well correlated with ethmoturbinal surface area, a known osteological correlate of olfactory function. This suggests that CPSA and FXSA are useful proxies for olfactory ability, especially when studying fossils or skulls in which turbinals are not preserved. Total area of CP foramina (FXSA), an exacting measure of olfactory nerve endocasts, is tightly correlated with CPSA. Because of this, it may be desirable to use CPSA alone as a proxy given that it is easier to measure than FXSA.
Anat Rec, 297:2080–2092, 2014. © 2014 Wiley Periodicals, Inc.

Key words: cribriform plate; olfaction; Carnivora; turbinal; turbinate; olfactory function

INTRODUCTION

We know little about the olfactory ecology of extinct mammals largely because we do not have an osteological proxy for olfactory ability that is likely to be preserved in fossils and that can be accessed without damaging specimens. Previous workers have relied on the relative size of the ethmoturbinal bones to infer olfactory function, or reliance on olfaction, in extant mammals (Allen, 1882; Negus, 1958; Maier, 1993; Maier et al., 1996; Smith et al., 2004; Van Valkenburgh et al., 2004, 2011; Green et al., 2012), but turbinals are fragile and rarely preserved in fossil skulls. A second possible metric, olfactory bulb vol-

Additional Supporting Information may be found in the online version of this article.

Grant sponsor: NSF Graduate Research Fellowship Program; Grant number: DGE-1144087; Grant sponsor: NSF; Grant numbers: IOB-0517748, IOS-1119768.

*Corresponding to: Deborah Bird, Department of Ecology and Evolutionary Biology, University of California, Los Angeles 90095, CA. Fax: 310-206-3987. E-mail: dbirdseed@gmail.com

Received 24 June 2014; Accepted 25 June 2014.

DOI 10.1002/ar.23032
Published online in Wiley Online Library (wileyonlinelibrary.com).

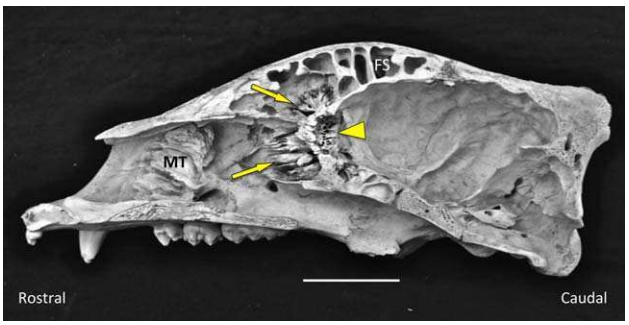

Fig. 1. Cribriform plate shown in the sagittally sectioned skull of a grizzly bear (*Ursus arctos)*. Arrowhead: Caudal aspect of cribriform plate. Arrows: ethmoturbinals; MT: maxilloturbinals; FS: frontal sinus. Skull courtesy of George Stevenson and Montana Fish, Wildlife and Parks. Scale bar: 5 cm.

ume, can be approximated from fossil cranial endocasts (Gittleman, 1991), but estimates may be unreliable, as the boundaries of the olfactory bulb cavity are inconsistent (Smith and Rossie, 2006). A third metric, the relative size of the cribriform plate (CP), is more promising. CP surface area has been shown to correlate with aspects of olfactory function (Bhatnagar and Kallen, 1974; Pihlström et al., 2005) and does preserve in fossils (Joeckel et al., 1997; Hoch, 2000; Kielan-Jaworowska, 2004; Garcia et al., 2007; Godfrey et al., 2013).

The CP, or lamina cribrosa, is a perforated cup of ethmoid bone that separates the nasal chamber from the olfactory bulb in mammals (Fig. 1). The myriad CP foramina are the only points of passage for axons from olfactory sensory neurons streaming from snout to brain and so provide an osseous imprint of peripheral olfactory innervation (Farbman, 1992). Tissue passing through the CP includes small amounts of connective tissue, circulating cerebrospinal fluid, and an occasional small vessel but is predominantly made up of axon fascicles (Doucette, 1991; Silver et al., 2002; Kavoi et al., 2010). For this reason, the CP and its foramina might be a reasonable proxy for the relative number of olfactory neurons transmitting information from the nose to the olfactory bulb (Paulli, 1900; Negus, 1958).

CP morphology, specifically its size and shape as well as the distribution, number and size of its foramina, varies markedly across mammalian taxa. It is the assumption of this article that the CP is an informative feature of olfactory anatomy, that aspects of the variation in CP morphology reflect differences in olfactory function (Allen, 1882; Negus, 1958). Olfactory capabilities of mammals can be defined in many ways and have been described variously as detection sensitivity (Marshall et al., 1981; Doty et al., 1984; Meisami, 1989), odor discrimination (Friedrich, 2006), and breadth of odor reception (Saito et al., 2004). For this study we have chosen to define olfactory capacity in terms of relative reliance on olfaction, something that can best be inferred from an animal's habitat and observed behavior (Kruuk, 1972; Estes, 1989; Ewer, 1998). Previous studies have begun to link CP morphology to ecology. It has been established that the CP, a trait unique to mammals, is secondarily reduced or lost altogether in obligate aquatic species. In the toothed cetaceans or Odontoceti, for example, the CP is present as anlage in the fetus but is entirely absent in the adult animal (Buhl and Oelschläger, 1988; Oelschläger, 1992, 2000; Colbert et al., 2005). Similarly, the adult mysticetes, or baleen whales, have lost all but a very rudimentary CP (Oelschläger, 1989). In the platypus (*Ornithorynchus anatinus*), an aquatic monotreme, the signature multitude of CP foramina has devolved into a single opening, while the closely related echidna (*Tachyglossus aculeatus*) maintains a fully formed CP (Kuhn, 1971; Zeller, 1988). Among terrestrial mammals, one clade known for its developed visual anatomy, the anthropoid primates, have exceptionally small CPs (Pihlström et al., 2005; Nummela et al., 2013). Diet may also be linked to CP morphology, as one comparative study of 40 bat species showed that frugivorous bats have a higher density of CP foramina than do insectivorous species (Bhatnagar and Kallen, 1974).

In order to clarify the relationship between CP morphology and behavioral ecology and infer the relationship between CP morphology and olfactory function in living and extinct species, we need to first establish rigorous, accurate methods of quantifying variation in the CP. Previous workers have focused on the surface area of the plate and number of foramina, using internal molds or direct measurements from sectioned skulls (Bhatnagar and Kallen, 1974; Pihlström et al., 2005). However, neither of these approaches is likely to be useful for fossil specimens. The CP is located in the anterior cranial fossa and can only be seen clearly by removing the calvaria, or skull roof. The cranial and nasal cavities of a fossilized skull are typically filled with matrix, making direct access to the plate even more problematic. Previous methods of studying CP size have additional limitations. Estimates of surface area calculated from linear measurements alone may be inaccurate, because CP shape is irregular and highly variable in most dimensions. Additionally, it is impossible to quantify the finer CP features, such as the total cross-sectional area of its foramina from direct measurements. However, the CP can now be visualized using computed tomography (CT) and imaging software, thus allowing quantification of variation in CP morphology, close examination of novel features, and the potential for studying olfactory anatomy in extinct taxa.

Before attempting to infer olfactory function in fossil mammals from CP surface area and/or foramina size and number, it is essential to understand the variation in these parameters across a broad sample of living species of known ecologies and body size. Not only do we need to know how CP size and foramina dimensions vary with body size and phylogeny, but we also need to understand the relationship among the three parameters: CP surface area, total cross-sectional area of CP foramina, and foramina count. This baseline information is needed to establish expected scaling relationships and thereby allow us to identify species that deviate from the expected, presumably due to olfactory adaptations.

Here, we present the first comparative analysis of CP morphology based on CT scans across a diverse sample of mammal species, all within the order Carnivora. We chose this order in part due to the ready availability of previously scanned skulls (Van Valkenburgh et al., 2004, 2011; Green et al., 2012), but also because carnivorans vary widely in body size and CP morphology and represent disparate ecologies with differing olfactory demands (Estes, 1991; Ewer, 1998; Wilson and Mittermeier, 2009).

TABLE 1. Sample species with associated skull length (orbit to occipital condyle length: OOL), cribriform plate surface area (CPSA), total cross-sectional area of CP foramina (FXSA), total number of CP foramina (NF), and olfactory turbinal surface area (OTSA)

Code	Species	Sex	OOL: orbit to occipital length (mm)	CPSA: CP surface area (mm^2)	FXSA: foramina cross-sectional area (mm^2)	NF: number of CP foramina	OTSA: olfact. turbinal surface area (mm^2)
MME	*Mephitis mephitis*	M	56.49	334.65		338	13374.8
		F	50.05	279.35	64.08	356	7153.8
ELU	*Enhydra lutris*	M	113.93	418.79	65.44	208	6182.24
		F	106.29	373.53	53.72	274	7523.26
GGU	*Gulo gulo*	M	103.6	889.60	146.12	454	71642.28
		F	100.78	813.88	150.16	502	52550.38
LCA	*Lontra canadensis*	M	87.14	223.29	56.06	328	8299.78
		F	89.24	280.77	55.78	410	10995.26
MFR	*Mustela frenata*	M	39.05	70.43	15.06	298	1695.08
		F	31.67	49.50	11.68	270	3018.24
NVI	*Neovison vison*	M	59.96	125.09	30.74	368	4713.96
TTA	*Taxidea taxus*	M	78.09	558.62			23246.96
		F	86.3	664.17	123.36	652	22955.14
PFL	*Potos flavus*	M	66.76	268.54	67.88	308	11385.12
		F	64.56	228.84	44.46	248	12854.3
PLO	*Procyon lotor*	M	75.53	353.08	66.00	314	19399.32
		F	77.94	412.00	85.74	394	22357.16
HLE	*Hydrurga leptonyx*	M	254.23	992.41	148.94	248	65081.22
		F	273.88	973.30			42075.5
MAN	*Mirounga angustirostris*	F	181.51	388.51	41.6	94	9189.19
MTR	*Monachus tropicalis*	M	187.09	510.89			21230.51
		F	170.38	406.99	50.02	86	18048.2
ZCA	*Zalophus californianus*	M	214.3	868.25	149.30	216	17527.7
		F	155.72	599.72	105.1	236	9323.76
UAM	*Ursus americanus*	M	196.6	1607.41	486.34	606	
		F	129.79	1339.36		590	72682.8
UAR	*Ursus arctos*	U	194.8	1467.82	487.618	826	
		F	205.65	2317.92		664	143929.5
UMA	*Ursus maritimus*	M	266.74	2800.14			254792
		F	232.1	2453.58	865.22	804	
CLA	*Canis latrans*	M	105.11	918.24	144.17	540	40071.5
		F	99.9	826.96	123.46	516	46420.34
CLU	*Canis lupus*	M	135.87	1045.53	194.126	572	116248.6
		F	122.37	946.09	193.704	578	
CME	*Canis mesomelas*	U	94.17	732.03	121.046		
CSI	*Canis simensis*	U	105.64	928.92	143.244		
LPI	*Lycaon pictus*	M	114.97	799.46	162.358	450	
		F	112.9	813.55	198.072	540	70391.68
NPR	*Nyctereutes procyonoides*	M	73.98	446.45	72.39	368	16364.9
		F	68.63	391.83	78.522	392	17934.82
OME	*Otocyon megalotis*	M	73.46	332.72	64.288	350	10671.5
		F	70.24	308.27	61.04	372	13394.84
SVE	*Speothos venaticus*	M	94.5	380.41	92.724	354	19668.1
UCI	*Urocyon cinereoargenteus*	M	73.72	290.80	46.24	352	10008.84
		F	73.46	296.33	61.44	428	13855.94
VLA	*Vulpes lagopus*	M	95.76	585.36	107	604	33182.98
		F	73.73	572.38	117.68	644	27662.68
VMA	*Vulpes macrotis*	M	64	349.05	62.28	612	12824.28
		F	76.43	356.02	69.778	646	14059.76
VVU	*Vulpes vulpes*	M	84.84	636.29	193.43	578	35840.3
		F	80.06	644.19	173.128	582	33264.32
CCR	*Crocuta crocuta*	M	155.53	1074.06	175.06	244	48966.68
		F	151.54	1157.79	165.70	260	73130.6
PBR	*Parahyaena brunnea*	M	146.46	1167.44	188.88	252	89789.1
		U	151.07	1322.74	172.538	196	99297.46
HHY	*Hyaena hyaena*	M	132.92	1057.66	235.428	240	64866.06
PCR	*Proteles cristata*	F	88.09	325.32	57.692	258	12361.48
GSA	*Galerella sanguinea*	M	48.53	101.82	26.44	206	2539.22
		F	46.14	87.25	18.58	170	1526.82
SSU	*Suricata suricatta*	M	40.55	81.05	17.58		1055.72
		F	41.52	95.30	23.94		1689.46
PPA	*Panthera pardus*	M	159.66	712.55	125.14	158	73781.4
LPA	*Leopardus pardalis*	M	98.76	293.326	83.184	192	21192.06

TABLE 1. (continued).

Code	Species	Sex	OOL: orbit to occipital length (mm)	CPSA: CP surface area (mm^2)	FXSA: foramina cross-sectional area (mm^2)	NF: number of CP foramina	OTSA: olfact. turbinal surface area (mm^2)
		F	100.92	315.17			
LRU	*Lynx rufus*	M	79.13	196.54	51.01	148	14852.92
		F	94.69	184.14	49.95	170	13479.12
AJU	*Acinonyx jubatus*	M	120.46	433.79	117.98	128	43846.78
		F	112.07	369.54	96.52	116	22123.96
PCO	*Puma concolor*	M	127.47	906.49	178.12	244	85849.7
		F	124.36	686.83	154.16	220	60988.42
FSY	*Felis silvestris*	M	67.27	178.51	43.81	214	11151.94
		F	62.45	145.75	37.56	178	6309.66
PLE	*Panthera leo*	M	209.79	1046.5	242.56	216	114745.3
		F	173.97	1041.53	219.42	264	79182.04
NNE	*Neofelis nebulosa*	M	120.58	479.04	84.942	112	

The code column is a guide to species abbreviations used to identify data points on the graphs in Figs. 7–9. Gaps in the data for the finer parameters (FXSA, NF) are due to the insufficient resolution of some existing scans.

Our study had four objectives, the first of which was to establish methodologies for quantifying three key features of CP morphology (CP surface area, total cross-sectional area of foramina, total number of foramina) using high-resolution CT scans and imaging software. This proved to be a significant challenge given the intricate and complex anatomy of CPs; a single foramen on the caudal aspect may represent the confluence of multiple foramina on the rostral aspect, and the level of CT scan resolution required to visualize such minute features was difficult to achieve in our largest skulls. Having measured the three parameters, our next objective was to study the relationship among them. Does foramina number or size increase linearly with CP surface area? Does one parameter predict another? Such questions are especially important in cases where features of the CP are damaged or scan quality is poor. Our-third objective was to understand how each of the parameters scaled with body mass, and our fourth was to explore the relationship between CP data and a previously established osteological correlate of olfaction, ethmoturbinal surface area. New methods secured from this study open the door to close examination of CP morphology in both fresh heads and fossil skulls embedded in matrix. While this article does not tackle questions of olfactory function, CP data gathered from animals representing divergent olfactory ecologies provide the basis for just such studies in the future.

MATERIAL AND METHODS

Sample

We sampled 77 skulls from 42 species and six families of carnivorans (Table 1). With the exception of the tropical monk seal (*Monachus tropicalis)*, all species are extant. The sample spans a wide range of body sizes (<1 to >500 kg) and represents a cross-section of behavioral ecologies. Availability permitting, we sampled two wild-caught adult specimens, one male, one female, for each species. Most skulls were scanned at the University of Texas High-Resolution CT Scanning Facility (http://www.ctlab.geo.utexas.edu). The field of view for each scan was restricted to the CP and surrounding ethmoturbinals in order to maximize resolution. Slice thickness ranges from 15 to 250 μm. Resolution for the large ursids was not sufficient to measure the small and complex CP foramina, so these species were rescanned on the phoenix v|tome|x s^{TM} scanner at General Electric Inspection Technologies Facilities (http://www.ge-mcs.com/en/inspection-technologies.html). Slice thickness was reduced and scan resolution improved, by an order of magnitude. All University of Texas scans are available through Digimorph (http://www.digimorph.org).

A three-dimensional digital model of the CP was made from each of the scans (Fig. 2). To do so, the scan was first imported into the visualization software package Mimics 15.0 (Materialise). A threshold was chosen that best delineated bone from nonbone. Using segmentation, bone that included the CP and the most posterior ethmoturbinals was selected and committed to a 2-D mask (Fig. 2B), which was then reconstructed as a 3-D model (Fig. 2C). Once rendered, these models could be rotated and magnified, allowing close access to any feature of the CP from any vantage point.

The first metric, CP surface area (CPSA), is defined here as the area of the CP perforated by olfactory foramina. It excludes the lateral section that is perforated only by the ethmoid foramen, a large passageway for the nasociliary branch of the trigeminal nerve. Establishing an accurate measure of CP bone surface within a complex latticework of openings is prohibitively difficult (Fig. 3A), so we first create a continuous surface in Mimics 15.1 using a wrapping function that fills the foramina in the 3-D model virtually (Fig. 2B). We import the wrapped model into a second imaging program, 3-matic 7.0.1 (Materialise) and select the area (Fig. 3C). Surface area is then isolated and calculated in 3-matic based on the number of triangles selected.

The second metric, total cross-sectional area of CP foramina (FXSA), is an estimate of the relative area occupied by peripheral olfactory nerves crossing the CP from snout to brain. We devised a unique metric that quantifies a surface not of bone but of missing bone. Specifically, we applied a "necklace" or spline of coordinate points along the perimeter of each foramen in the 3-D model (Fig. 4B). Splines from all foramina are imported into Rhinoceros 4, a NURBS-based 3-D modeling software (McNeel and Associates). Rhinoceros then calculates the area of each foramen as a nonplanar

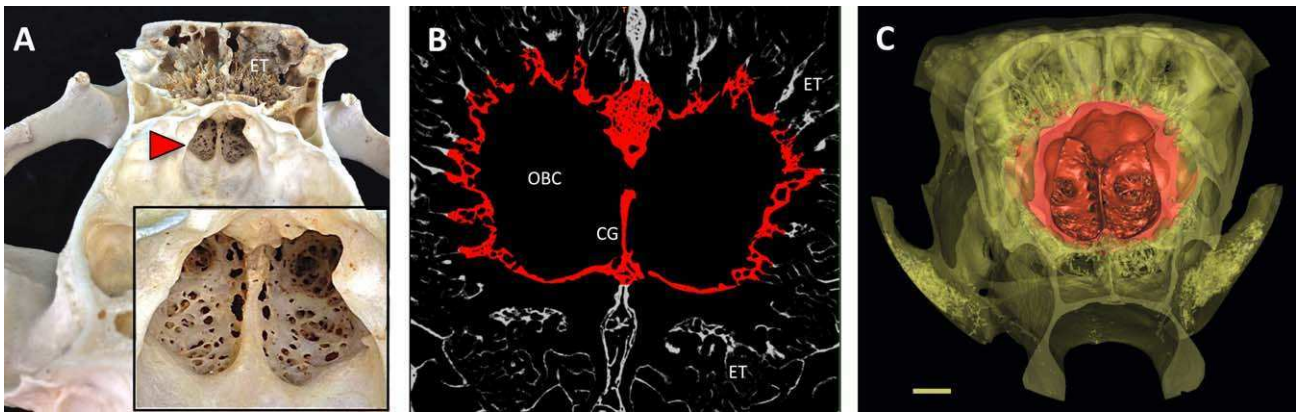

Fig. 2. Cribriform plate (CP), from bone to digital reconstruction. (**A**) Skull of grizzly bear *(Ursus arctos)* with calavaria removed, viewed from caudal aspect. Arrowhead: CP. Inset: close-up of caudal surface and foramina of CP. (**B**) Segmentation: CT scan of CP and surrounding turbinals (in coronal view) is imported into Mimics 15.0; CP bone (red) is selected and committed to 2-D mask. Scan produced on phoenix v|tome|x s^{TM} high-resolution scanner. (**C**) Reconstructed 3-D model of CP (red) seen from caudal aspect inside skull matrix (yellow). CG: crista galli; ET: Ethmoturbinals; OBC: olfactory bulb cavity. Scale bar: 1 cm.

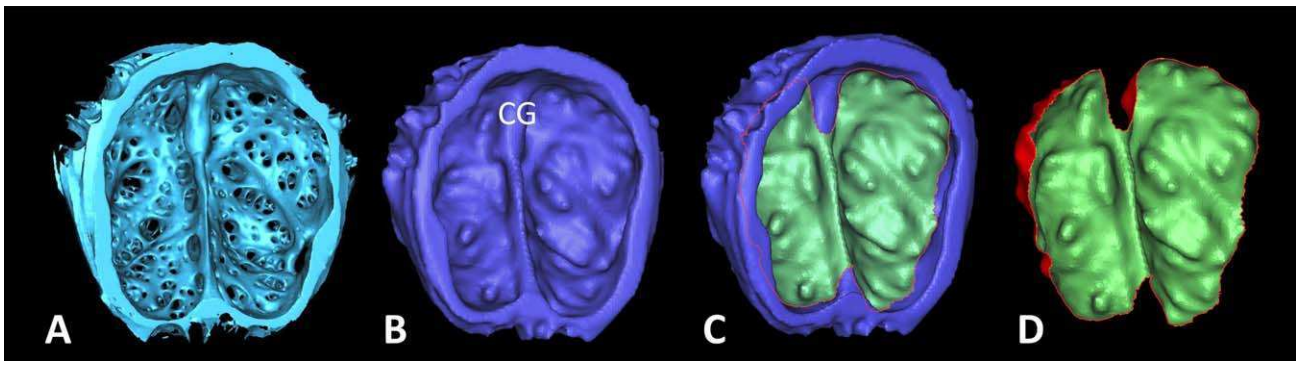

Fig. 3. Measuring CP surface area. (**A**) 3-D CP model from North American river otter (*Lontra canadensis)* made in Mimics 15.0, as viewed from caudal aspect. (**B**) A continuous surface is created in Mimics by virtually filling foramina with a wrap function. (**C**) Wrapped model is imported into 3-matic 7.0.1. Surface area of perforate zone in CP is selected. (**D**) CP surface is isolated and area calculated. CG: Crista galli.

surface between coordinate points within a voxel matrix and then totals them, giving us FXSA (Fig. 4C). In nearly all cases, splines were applied to single foramina, but wherever one foramen on the caudal aspect was made up of several foramina feeding into it from the rostral side, the single, caudal-most foramen was measured (Fig. 4B). This ensured that the cross-sectional area was measured at the narrowest passage through the bone, this being the maximum diameter available for nerve tissue crossing the CP at this point. Of our three metrics, FXSA is perhaps the closest representation of olfactory nerve bundles, but it presents two practical limitations. In addition to being time-intensive, measuring FXSA requires extra high-resolution scans. Due to the uneven quality of some of our older CT scans, FXSA data do not exist for some specimens in our sample.

To count the total number of CP foramina (NF) in each specimen, we assigned numbered points to each opening on the 3-D model and totaled these. Perforation patterns differ among species. In most cases a single opening guides a single axon bundle through the bone, but in some animals a single opening is made up of multiple foramina, all housing smaller nerve bundles that converge from anterior to posterior. Wherever the latter was the case, all converging foramina were counted (Fig. 4A).

The body size proxy used for this study was skull length as described by the distance between the anterior extent of the orbit to the posterior extent of the occipital condyle (OOL). We chose skull length over body mass because our sample included pinnipeds whose body mass is exaggerated due to their large stores of fat. Additionally, our skull length metric (OOL), which includes only the cranium, avoids the confounding effect of highly variable snout lengths among our sample species, particularly an issue among felids and canids (Van Valkenburgh, 1990). Basicranial length is often used for this same purpose. We chose to not use this metric, as it relies on sutures as its boundaries, and sutures are often fully fused and thereby difficult to delineate in adult mustelids. Skull length (OOL) was measured on 3-D digital models of full skulls. Where full skull scans

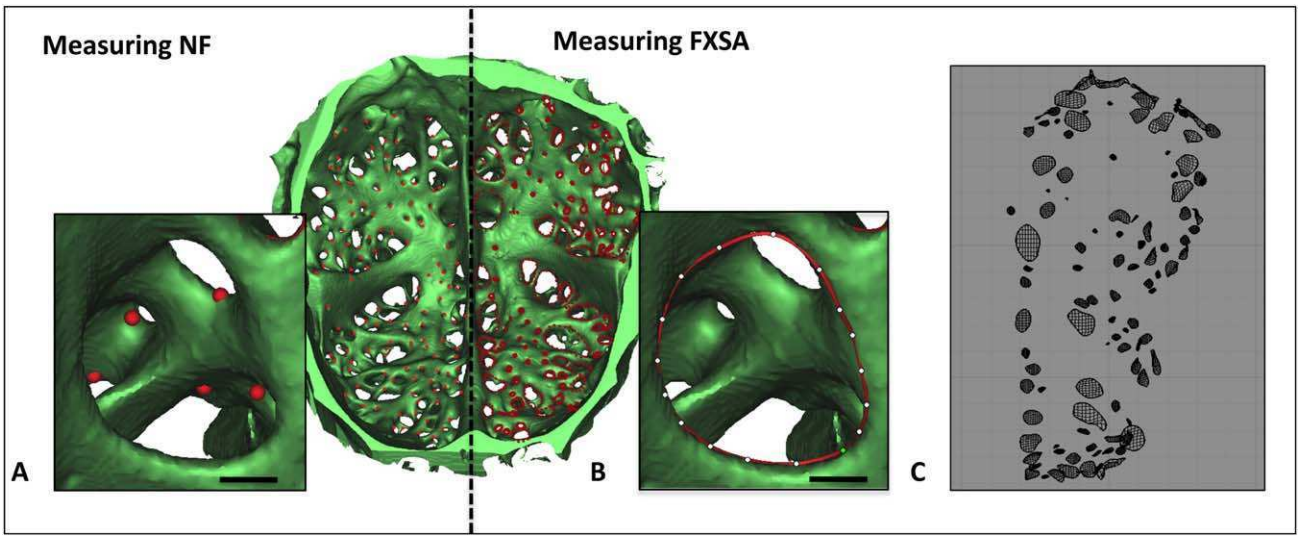

Fig. 4. Measuring foramina on a digital model of an American mink *(Neovison vison)* cribriform plate made in Mimics 15.0. Left side**:** Numbered points are assigned to all openings to quantify total number of foramina (NF). (Inset **A**) If multiple foramina converge onto a single opening, all foramina are counted. Right side: Coordinate points in a voxel matrix (splines) are drawn along the perimeter of all openings to measure foramina cross-sectional area (FXSA). (Inset **B**) if a single foramen is made up of several feed-ins, it alone is measured. Scale bar for Inserts A and B: 20 μm. (**C**) Splines are imported into imaging program Rhinoceros 4.0 where nonplanar surface areas are calculated and tallied.

did not exist for specimens, OOL was measured directly from the skulls with mechanical calipers. To test consistency, we applied both methods to two different specimens and found no significant difference.

Finally, estimates of olfactory turbinal surface area (OTSA) used in this study are taken directly from published data (Green et al., 2011; Van Valkenburgh et al., this volume). In these articles as well as ours, olfactory turbinals are defined to include the nasoturbinal bones as well as all ethmoturbinals and frontoturbinals located outside the respiratory pathway.

Statistical Analysis

Species means were derived for FXSA, NF, CPSA and olfactory turbinal surface area (OTSA) as well as the body size proxy, OOL. With the exception of the number of foramina (NF), all species means were log transformed to normalize the data. To view the scaling relationships between the CP features and body size, each CP measure was plotted against OOL. Linear regressions between each of the olfactory variables were performed to determine whether the CP and turbinal data reinforce each other. In all cases, generalized least squares (GLS) regressions were performed in R (R Code Team, 2012).

To account for phylogenetic relatedness and covariance among taxa, we constructed a time-calibrated phylogeny specific to this study. For this, we trimmed taxa from a recently constructed Carnivora phylogeny (Slater and Friscia, unpublished), an extension of the caniform phylogeny published by Slater et al. (2012). We then performed phylogenetic generalized least squares (PGLS) analyses (R Caper package) to reexamine relationships between all variables. If CP morphology has evolved under the significant influence of phylogeny, we expect that Pagel's lambda will not be significantly different from one. As all of the variables are shown to be under strong phylogenetic influence, slope and correlation r^2 values reported in the text are derived from regressions in which phylogeny is accounted for (PGLS). For visualization purposes, however, GLS plots are shown in Figs. 7–9.

RESULTS

Qualitative Observations

Using high-resolution CT scans and imaging software we transformed the CPs of 76 carnivorans into discrete digital 3-D models within virtual skull matrices. Visible from every vantage point and measurable with new digital applications, these 3-D reconstructions give us an accurate picture of the gross and fine comparative anatomy of the CP. Close examination of the 3-D models allowed us to define general features of CP morphology in Carnivora. In all specimens observed, the CP can be described as a perforated concavity in the ethmoid bone at the posterior most extent of the nasal cavity. Struts of imperforate bone reinforce the perforated surface from lateral to medial. On the rostral aspect, the plate is bisected along the midline by the perpendicular ethmoid bone of the nasal septum, on the caudal side by the crista galli. On either side of the crista galli is a distinctly linear series of large foramina (Fig. 5). Generally, one or two pairs of these medial most foramina open into deeper tunnels of bone that project into the nasal chamber. Multiple foramina converge from anterior to posterior into these paired tunnels. The location of these tunnel-like foramina within the dorsal half of the CP is intriguing because it matches early illustrations and descriptions of the specific point at which axon bundles streaming from the vomeronasal organ cross from the nasal septum to the cranium (McCotter, 1912).

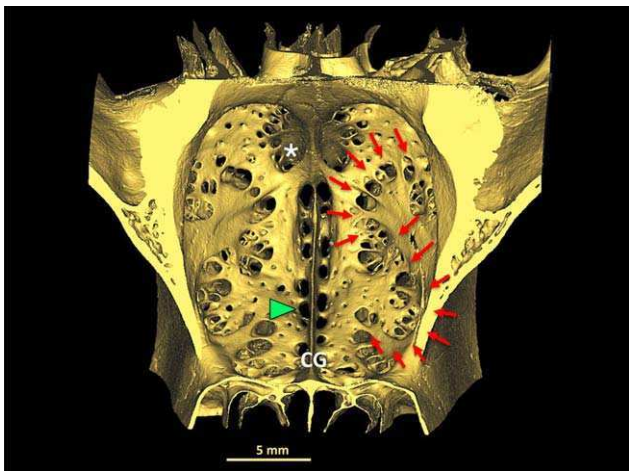

Fig. 5. Foramina distribution patterns shown in an aardwolf *(Proteles cristata)* cribriform plate. The crista galli (CG) divides the CP bilaterally. Two rows of foramina line either side of midline in all carnivoran CP (green arrowhead). Cribriform plates are often perforated along the dorsomedial midline by a pair of deep tunneling foramina (asterix). These openings extend rostrally in osseous canals that straddle the perpendicular ethmoid plate of the nasal septum. All feliform CP share a sigmoidal pattern of foramina (red arrows).

Determining with certainty whether any of the CP foramina are dedicated exclusively to vomeronasal nerves will require concurrent dissection and modeling of CP from fresh heads in a future study.

Several general patterns of variation in CP morphology stood out in our initial qualitative observations of the 3-D models. In contrast to its enduring description as a plate, CP shape appears in fact to be highly variable in all dimensions. Within the constraints of bilateral symmetry, the shape defined by the caudal surface area of the CP is irregular and ranges from deep (anterior to posterior) and roughly spherical in the polar bear (*Ursus maritimus)* to shallow and kidney-shaped in the elephant seal (*Mirounga angustirostris)*, showing just two examples (Fig. 6A-C). The crista galli, a ridge marking the division between the two lobes of the olfactory bulb (OB), is morphologically diverse as well. Wide enough to fully separate the OB lobes in the elephant seal (Fig. 6B), the crista galli is nearly absent in some carnivorans, such as the slender mongoose (*Galerella sanguinea)*. Perhaps the most variable aspect of CP morphology is the pattern of its perforations, that is, the size, number and distribution of its foramina. Qualitative observations suggest that CP in closely related species tend to have similar patterns of foramina distribution. Canid CP, for example, appear to have a characteristically dense distribution of foramina, many of which are relatively small, while feliform plates share a lower density pattern of larger holes distributed in a sigmoidal pattern along its lateral aspect (Fig. 5). In exceptional cases, closely related species have markedly different CP shape and foramina distribution. For example, the contrast between the wolverine's (*Gulo gulo*) deeply cupped, highly perforated CP and the flattened, sparsely perforated plate of the sea otter (*Enhydra lutris*) likely reflect differences in olfactory capacity and/or skull shape constraints.

Scaling CP Metrics With Body Size

Inferring olfactory function from our three CP metrics is beyond the scope of this article, but as a first step in this direction, we examine the scaling relationships between each of the variables and body size. The total area of the CP foramina (FXSA) scales to our body size proxy, orbit to occipital condyle length (OOL), with negative allometry ($r^2 = 0.67$, slope = 1.70). The slope is significantly less than expected under geometric similarity and indicates that larger animals have relatively smaller CP for their size (Fig. 7A). Surface area (CPSA) appears to scale to OOL ($r^2 = 0.77$) with slightly less negative allometry and a slope of 1.80 (Fig. 7B). Much of the noise, or scatter in these two plots can be attributed to the low CPSA and FXSA values for the phocid pinnipeds, the elephant seal (MAN, *M. angustirostris*), tropical monk seal, (MTR, *Monachus tropicalis*) and leopard seal, (*HLE, Hydrurga leptononyx*), and very high FXSA values for the grizzly bear (UAR, *Ursus arctos*), polar bear (UMA, *Ursus maritimus*), black bear (UAM, *Ursus americanus*) and red fox (VVU, *Vulpes vulpes*; Fig. 7A,B). Scatter is more pronounced for FXSA than CPSA, particularly evident in the spread between the largest caniforms, the pinnipeds and ursids (Fig. 7A). In both FXSA and CPSA plots, the caniforms tend to ride above the regression line with the exception of the aquatic and semi-aquatic species. In contrast, the feliforms tend to fall below the regression line with the exception of the three carnivorous hyaenids (CCR, HHY, PBR) and the mountain lion (PCO, *Puma concolor*). Finally, among our three metrics, total number of CP foramina (NF) stands out for its weak relationship to skull length ($r^2 = 0.15$, $P = 0.007$). Disregarding the scant correlation to skull length, we can see that absolute NF values separate caniforms into aquatic and nonaquatic in concordance with the other two parameters, but that in contrast to FXSA and CPSA, NF values rank all feliforms together as sharing CP morphology with relatively few perforations (Fig. 7C).

Relationships Among the CP Metrics

Each of the three CP variables was viewed in relationship to one another.

What first stands out among these comparisons is the strong positive correlation between CPSA and the totaled area of its foramina (FXSA), with 90% of the variation in FXSA explained by CPSA (Fig. 8A). CP surface area predicts the total area of its foramina. Interestingly, some of the same species deviate from the expected as those that do when FXSA is regressed against skull length, two ursids (UAM, UMA) and two phocid pinnipeds (MAN, MTR). Plotting the total number of CP foramina (NF) against CPSA (Fig. 8C) shows a far weaker, yet significant, relationship ($r^2 = 0.30$ $P < 0.001$). A slightly stronger correlation exists between NF and FXSA, with approximately 35% of the variation in NF

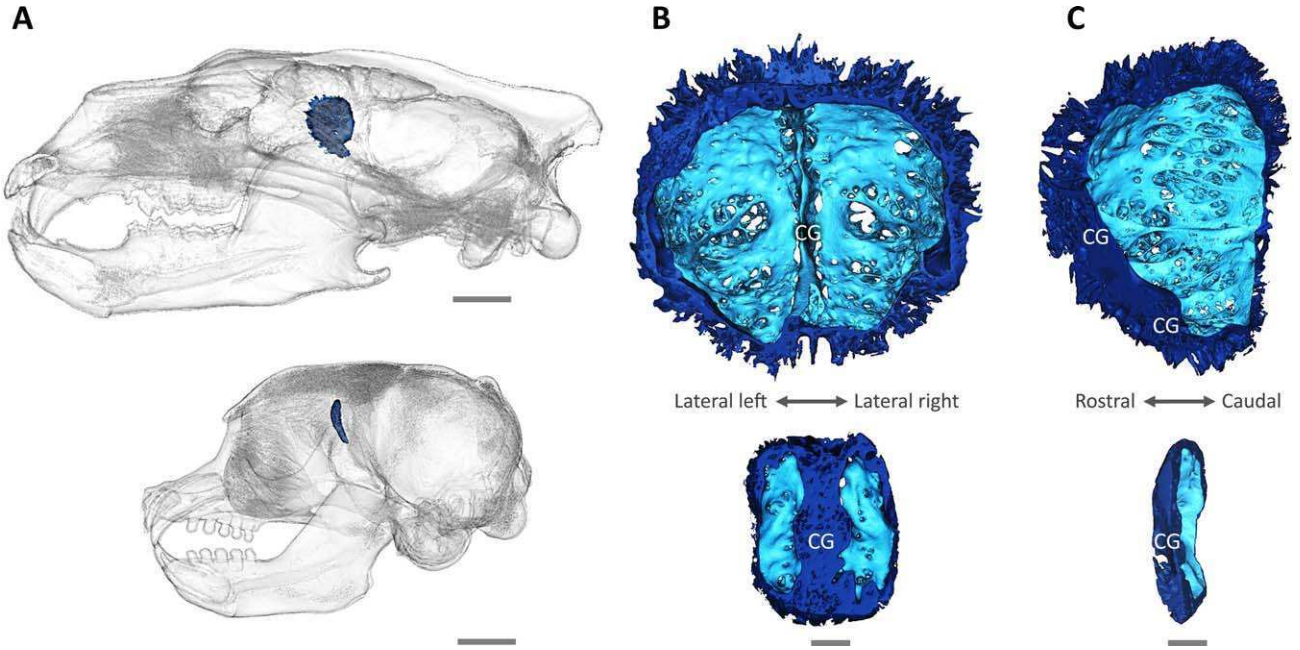

Fig. 6. Examples of CP shape variability. Top row: polar bear *(Ursus maritimus*); bottom row: elephant seal *(Mirounga angustirostris)*. (Left column **A**) Cribriform plate (dark blue) viewed within the skull. (Middle column **B**) Caudal view of CP showing the concave housing for the olfactory bulb. Dark blue: rostral aspect of plate with attached turbinal fragments; light blue: caudal CP surface. Polar bear CP (top) is 23.22 mm at its widest from crista galli to lateral extent. Elephant seal (bottom) CP is 5.56 mm at its widest from crista galli to lateral extent. (Right column **C**) Sagittally sectioned CP as viewed from the midline (CG: crista galli). The polar bear CP cavity is deep (24.66 mm rostral-caudal) and roughly semispherical; the elephant seal CP is shallow (7.72 mm rostral-caudal) and roughly kidney shaped. Irregularity in CP shape suggests that CP surface is more accurately captured by digital methods than previous linear measurements. Scale bars: (A) 20 mm; (B, C) 5 mm.

explained by FXSA (Fig. 8B). In both NF plots, all feliforms, including the hyaenids, tend to group with the aquatic caniforms as having reduced NF relative to the terrestrial caniforms (Fig. 8A,B).

Olfactory Turbinals

Finally, we investigated the relationship between the CP and an established osteological correlate of olfactory capacity, the ethmoturbinal surface area (Van Valkenburgh et al., 2004, 2011; Green et al., 2012). Developmentally related as two components of one ethmoid bone (De Beer, 1937; Rowe et al., 2005), the CP and the ethmoturbinals are functionally connected as well. Scrolls of turbinal bones on the anterior surface of the CP are covered in part by olfactory epithelium, a carpet of olfactory sensory neurons that send fascicles of axons through the CP foramina to the brain. For our PGLS regressions we use published data on the total surface area of fronto-ethmoturbinals and nasoturbinals in carnivorans (OTSA; Van Valkenburgh et al., 2004, 2011; Green et al., 2012). Among our regressions we find a tight correlation between total foramina area (FXSA) and OTSA ($r^2 = 0.87$, Fig. 9A). Ursids stand out as having higher FXSA than might be expected from the turbinal data. A very similar tight relationship exists between CP surface area (CPSA) and OTSA ($r^2 = 0.88$, Fig. 9B). Here, the California sea lion (ZCA, *Zalophus californianus)* is anomalous with an unexpectedly large CP surface area in relationship to OTSA. We can conclude that both FXSA and CPSA can be estimated from olfactory turbinal surface area in these carnivorans. CP surface area and FXSA scale to OTSA with strong negative allometry (Table 2). This relationship might be expected, as FXSA and CPSA more directly represent the presence of olfactory tissue than OTSA (turbinals are only partially covered in olfactory epithelium), and because sensory tissue is known to scale with extreme negative allometry across large body size ranges (Jerison, 1973; Menco, 1980; Nummela, 1995). Of the three CP variables, number of foramina (NF) has the weakest relationship to turbinal surface area, with only 36% of the variation in NF explained by turbinal surface area (Fig. 9C). This mirrors the previous pattern in which NF is decoupled from other CP metrics (Fig. 8B,C).

DISCUSSION

Qualitative Observations

Often the stepchild of olfactory anatomy, the CP is rarely described in the literature (Allen, 1882; McCotter, 1912; Radinsky, 1969; Kuhn, 1971; Wall, 1980; Rowe et al., 2005; Zeller, 1988; Smith and Rossie, 2006). Even rarer are comparative studies of specific features of CP morphology over a large number of taxa (Bhatnagar and Kallen, 1974; Pihlström et al., 2005). Results from the present study have created the basis for consistent, close examination of CP morphology across many species of living as well as extinct mammals. Our study confirms that variation in CP morphology is pronounced and that this variation is measurable using a nondestructive, digital approach. Novel methods established in our study

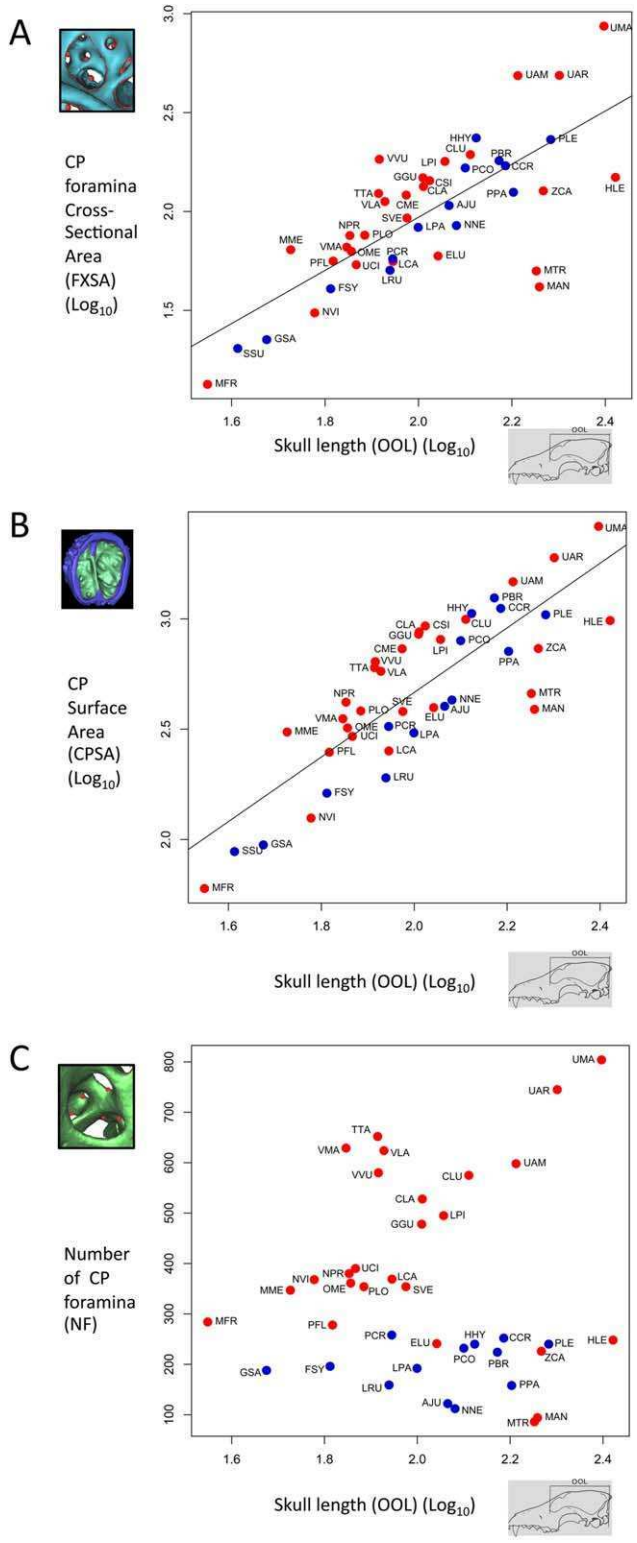

Fig. 7. Generalized least squares regression plots of cribriform plate (CP) parameters against estimated body size. Skull length (orbit to occipital condyle length: OOL) is used as a proxy for body size. All parameters in (A)–(C) are $\log_{10}$-transformed with the exception of number of foramina (NF). Red circles are caniforms; blue circles feliforms. See Table 1 for species codes and Table 2 for summary statistics.

enabled both full visualization of CP gross anatomy and the quantification of its finer-scaled features. This work was performed on 42 carnivoran species of known ecologies and body size as a first step toward establishing CP metrics as proxies for olfactory function.

Our general observations of CP gross anatomy contradict earlier assumptions about CP shape. Beyond shared bilateral symmetry and concave caudal surface, CP shape does not appear to be generalizable. This has a bearing on which methods most accurately measure CP size, specifically CP surface area. Previous estimates of CP surface area, calculated from linear measurements alone, relied on an assumption that the CP could be summarized as an oblate ellipsoid (Pihlström et al., 2005). Our CPSA values were consistently higher than Pihlström et al.'s among the 17 species found in both our studies, with increases ranging from a factor of 0.25–1.57. One might expect this, as measurements taken from digital reconstructions account for the specific shape profile of each CP, while linear estimates are derived from equations that fit a single gross shape. While we do not attempt to quantify shape differences in this article, it is evident from initial examination of 77 CP models made from CT scans that CP morphology is irregular in all dimensions and as such is most accurately quantified using a digital approach.

The CP belies its given name. It is far from flattened or plate shaped. Instead it has dimensionality. In some species, as in the ursids, the CP is a pronounced concavity while in others it is a shallower trough. But in all cases it is a kind of cup surrounding the olfactory bulbs. If anything, the CP might be better named "cribriform cup" or "cribriform calyx."

Establishing Digital Methods

With the aid of CT scans and imaging software, we designed digital methods that made possible for the first time nondestructive quantification of two features of CP morphology, the number of CP foramina (NF) and their cumulative cross-sectional area (FXSA). One previous study successfully counted CP foramina in 40 bat species, but because of the limitations of direct measurement, the cryptically located CP had to first be removed, thereby compromising the future research potential of the skulls (Bhatnagar and Kallen, 1974). Likewise, an earlier effort to quantify the area of CP foramina was restricted to an analysis of photographs taken from sectioned skulls (Kalmey et al., 1998). In contrast to both of these methods, we used as our reference digital 3-D models of CPs rendered directly from the voxel matrices of CT scans. In this way, CP foramina were measured from coordinate points we placed along the perimeter of each opening within the model, a method that can be performed on a large number of animals with no damage to the original specimens. The nondestructive methods developed in this study for visualizing and quantifying all dimensions of CP foramina are a necessary advance if we are to conduct comparative studies on CP morphology from museum specimens, rare species and fossils.

Relationship Among Three CP Metrics

If we expect variation in CP morphology to reflect aspects of olfactory capacity, as is asserted in the

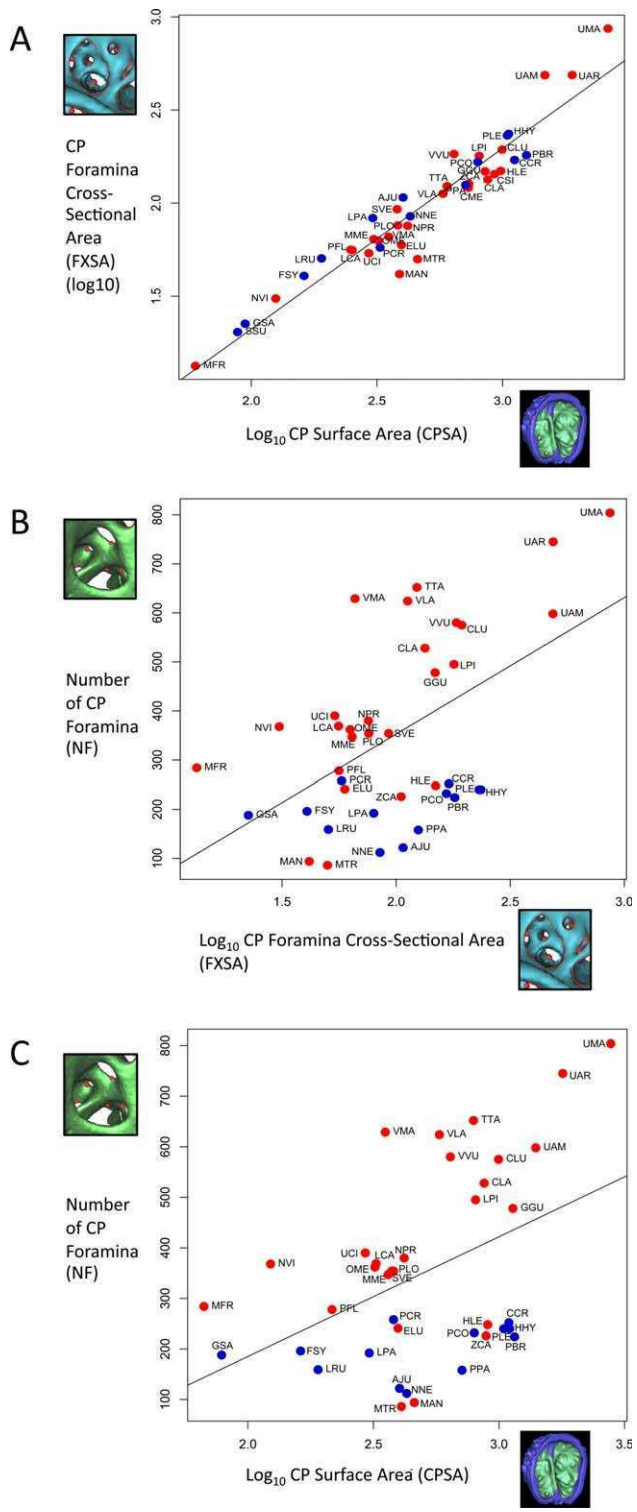

Fig. 8. Pair-wise regression plots of three cribriform plate (CP) metrics. Surface area variables (FXSA, CPSA) are $\log_{10}$-transformed; number of foramina (NF) is not. Red circles are caniforms; blue circles feliforms. See Table 1 for species codes and Table 2 for summary statistics.

literature (Negus, 1958; Bhatnagar and Kallen, 1974; Kalmey et al., 1998; Pihlström et al., 2005), we might in turn expect the three variables measured in this study, CPSA, FXSA and NF, to be strongly correlated and to predict one another. In fact, the relationships between the three metrics are not equally strong. While the metrics all reinforce each other, the only truly predictive relationship is between CP surface area and foramina cross-sectional area with 90% of the variation in FXSA explained by surface area. The relationship between NF and the other two variables is significant but far weaker. The strong correlation between CPSA and FXSA is notable for several reasons. First, as a collective endocast of the nerve fibers coursing through the CP, FXSA might be considered to be a more direct representation of peripheral olfactory innervation and function, and as such a more informative metric than either CP surface area or olfactory turbinal surface area. Supporting this is the fact that material contained in CP foramina is made up almost exclusively of nervous tissue, specifically olfactory axon fascicles, ensheathing cells, cerebrospinal fluid, and an occasional very small vessel (Doucette, 1991; Farbman, 1992; Silver et al., 2002; Kavoi et al., 2010). Relative size of axon bundles crossing the plate corresponds to the area and density of olfactory sensory neurons (OSN) found on the olfactory nasal epithelium, and in turn, OSN density is known to determine olfactory sensitivity (Apfelbach et al., 1991; Kandel et al., 2000). With its direct relationship to olfactory nerve tissue, FXSA might be viewed as a more rigorous metric of olfactory function than plate size. Whether this is the case remains to be tested in future functional studies, but it is evident from this study that the finer-scaled FXSA reinforces the coarser-scaled CPSA across our entire sample of carnivorans. Second, this strong relationship between FXSA and CPSA is important when considering undertaking large-scale comparative studies of CP morphology. In contrast to the relatively simple steps of determining CP surface area, securing an accurate measurement of the cumulative foramina area is a labor- and time-intensive process that demands particularly high-resolution scans. Such scans can be expensive and data-rich as well, making them somewhat cumbersome to work with. Our results here suggest that in future studies we can rely largely on quantifying CPSA and reinforce this with FXSA quantification in a smaller number of specimens. This is the approach we are currently using in a study we have begun on the relationship between CP morphology and olfactory gene repertoire, in which a number of the sample species, such as the armadillo (*Dasypus novemcinctus*) and cow (*Bos taurus)*, have exceptionally intricate and numerous foramina. Finally, and most importantly, our results indicate that when we apply our methods to CP morphology in fossils, CPSA can be substituted for FXSA wherever plates are damaged or foramina obscured by matrix.

The weak relationship between NF and the other two variables confounds any easy assumption that the total number of CP foramina alone predicts olfactory ability. The relationship between NF and FXSA makes sense in light of the general perforation patterns observed in the CP. Not all foramina are created equal. For example, in our study, wherever numerous rostral openings converged onto a single caudal foramen, we counted all

TABLE 2. Summary statistics for phylogenetic least squares regressions between all parameters

Regression	Analysis	r^2	Slope	*P* value	Pagel's lambda	Lambda lower bound = 0	Lambda upper bound = 0
FXSA vs. OOL	PGLS	0.67	1.7	<0.001	0.96	<0.001	0.35
CPSA vs. OOL	PGLS	0.77	1.8	<0.001	1.00	<0.001	1.00
NF vs. OOL	PGLS	0.15	284	0.007	1.00	<0.001	1.00
FXSA vs. CPSA	PGLS	0.90	0.93	<0.001	0.64	0.02	0.003
NF vs. FXSA	PGLS	0.35	201	<0.001	1.00	<0.001	1.00
NF vs. CPSA	PGLS	0.30	198	<0.001	1.00	<0.001	1.00
FXSA vs. OTSA	PGLS	0.87	0.68	<0.001	0.60	0.015	<0.001
CPSA vs. OTSA	PGLS	0.88	0.69	<0.001	1.00	0.001	1.00
NF vs. OTSA	PGLS	0.36	155	<0.001	1.00	<0.001	1.00

All correlations were significant at the 0.05 level. Pagel's lambda values are relative measures of phylogenetic influence on the data, ranging from zero (no influence) to one (strongest influence). Lower and upper bound *P* values indicate whether lambda values are significantly different from lower bound zero or upper bound one. Phylogeny has a strong influence on all parameters.

foramina toward the NF total but we only measured the caudal-most foramen for the FXSA total, as this foramen area best describes the space constraint for axons crossing the CP at this particular point. Two equal cross-sectional areas can be comprised of one or many foramina.

Using NF as a proxy for olfactory function proves to be problematic for two additional reasons. In some species, especially within the nonaquatic caniforms, there is a small swath of bone in the CP perforated by unusually small foramina (on the order of 10–25 μm in diameter). Whether these particularly small foramina serve a function separate from axon transport, such as drainage of cerebrospinal fluid (Silver, et al., 2002), remains to be seen and can only be solved with a much needed histological examination of the CP. These myriad little perforations amount to negligible cross-sectional area but contribute a sizable number to NF total and so partially account for an inflated NF relative to FXSA in terrestrial caniforms (Fig. 8B). This problem might be alleviated by not counting foramina under a certain size. There was a second obstacle to collecting consistent NF data. Because the smallest foramina can only be visualized in scans of very high resolution, it is possible that foramina in some specimens were undercounted solely due to inadequate scan quality. Intraspecific variation was pronounced in our NF results and may be attributable to this issue. This can only be tested by conducting a future CP study across a number of individuals of a single species.

The relationship between total number and total area of CP foramina is particularly weak within the feliforms. On the one hand, NF in all four species of hyaenids is similar to that among fellow feliforms, in which all share a common pattern of low foramina density. But in their FXSA and CPSA, the three carnivorous hyaenids rank among the canids and stand apart from other feliforms, even their own closest relative, the insectivorous aardwolf (Fig. 7A,B). This suggests that NF is determined by phylogeny, as much or more than function. High lambda values in all PGLS regressions involving NF suggest this may be the case (Table 2), but this needs further investigation.

Relationship Between CP and Olfactory Turbinals

To test assumptions that CP morphology reflects olfactory function (Negus, 1958; Bhatnagar and Kallen, 1974; Pihlström et al., 2005) we viewed all three CP metrics in relationship to an established osteological correlate of olfactory capacity, olfactory turbinal surface area (Van Valkenburgh et al., 2004, 2011; Green et al., 2012). Results show a tight correlation between olfactory turbinal surface area and two of the CP metrics, suggesting that both CP surface area (CPSA) and foramina cross-sectional area (FXSA) might be used as additional proxies for olfactory capacity. When conducting comparative studies of olfactory function among living mammals, it might be preferable to consider all aspects of nasal skull morphology, turbinals as well as CP features, but among extinct mammals this is rarely an option. Fragile turbinals are most often broken or missing in fossils skulls, leaving the relatively robust CP as the best-preserved feature of olfactory skull morphology. Our results show a strong correlation between olfactory turbinal surface area and CP surface area and foramina, reinforcing the prospects of studying olfactory function from fossils in which turbinals are destroyed and only the CP is intact.

Future Work

This study examined scaling relationships for the three CP metrics to skull length as a way to begin evaluating how CP morphology varies across species. The variation in CP morphology evident in Fig. 6A–C will be tested against what we know about the olfactory behavior, ecology and genomics of species. Using parameters established in this study, we will compare CP morphology in ecological groupings that reflect a spectrum of olfactory demands, such as aquatic and terrestrial species. Already our results appear to differ sharply from conclusion drawn by Pihlström and colleagues, from their 2005 study, that the CP surface area of the pinniped species in his sample do not markedly deviate from that of terrestrial mammals. The data from our article need further analysis to quantitatively test this conclusion. As a way of comparing olfactory behavior we will study the CP morphology among predators that use disparate hunting strategies, one more reliant on scent (for example, canids) and the other on sight (for example, felids). Finally, we are beginning to explore the relationship between the olfactory genomics and CP morphology in mammal species whose olfactory gene repertoires are known (Olender et al., 2003; Niimura and Nei, 2005, 2007; Kishida et al., 2007; Hayden et al., 2010).

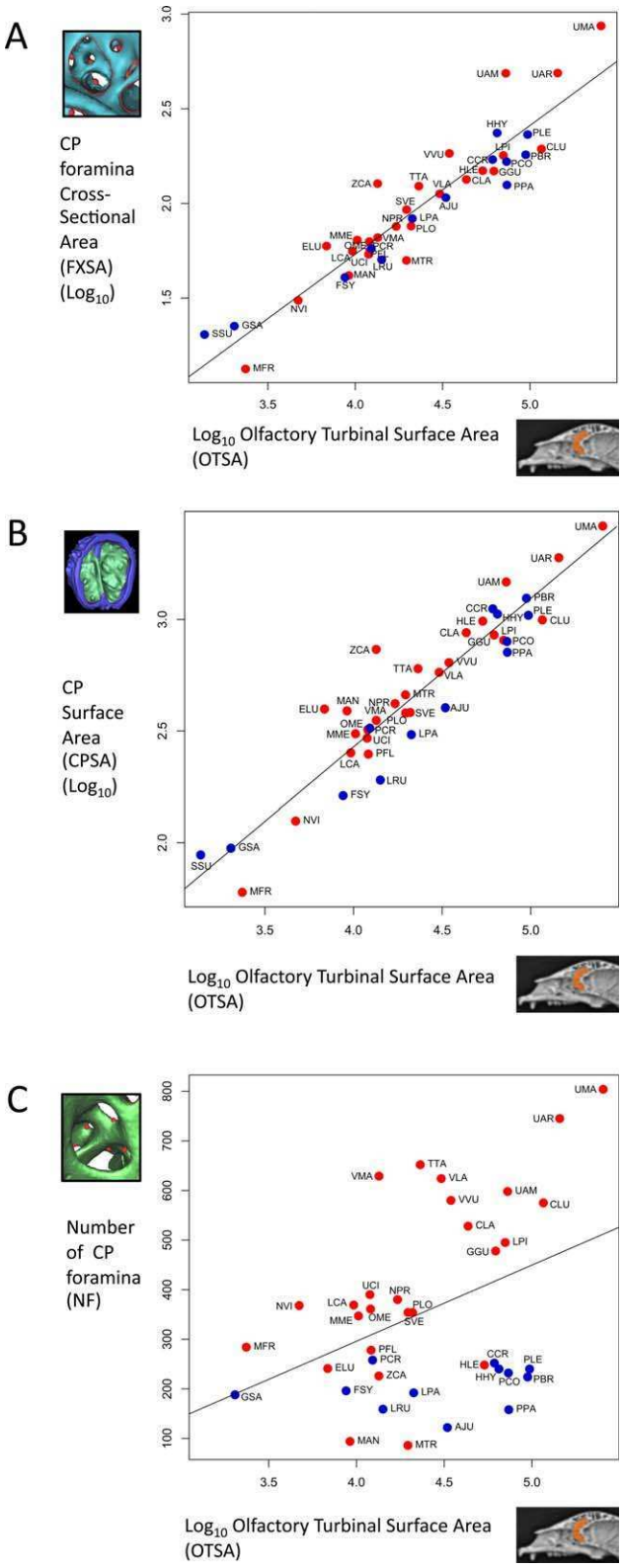

Fig. 9. Generalized least squares regression plots of cribriform plate (CP) parameters against olfactory turbinal surface area (OTSA). Surface area variables (FXSA, CPSA) are log_{10}-transformed; number of foramina (NF) is not. Red circles are caniforms; blue circles feliforms. See Table 1 for species codes and Table 2 for summary statistics.

A sense of smell is critical for most mammals. Olfactory systems have evolved to operate in distinct ecologies: as lineages, landscapes and chemical stimuli change over evolutionary time, species have acquired and lost particular traits of olfactory anatomy. Living animals offer us tissue with which to study these gathered olfactory adaptations, extinct species only the imprint of that tissue in the bone. Yet this bone is informative. The CP is the only feature that explicitly documents the trail left by olfactory nerves. This trail is quantifiable and comparable across extant species whose olfactory behavior and genomics we can witness. If such functional studies in living mammals establish CP morphology as a proxy for olfactory capacity, we can use novel digital methods developed in these study to examine CP features in detail in fossils. In this way, CP morphology might offer us a new osteological insight into the olfactory ecology of extinct animals.

ACKNOWLEDGMENTS

We thank M. Colbert, R. Ketcham, and J. Maisano of the University of Texas HRCT Digital Morphology group for their skill and care in producing CT scans, M. Faillace, R. Rudolph, and J. Urbanski of General Electric Inspection Technologies for their assistance, patience, and precision in producing high-res CT scans, George and Jana Stevenson for the loan of bear skulls, curators, and collection managers who lent us skulls; for scanning, G. Slater and A. Friscia for their carnivoran phylogeny, and finally L. Rosales, Y. Davydov, N. Goody, and P. Green for their cumulative years of data collection.

LITERATURE CITED

Allen H. 1882. On a revision of the ethmoid bone in the Mammalia, with special reference to the description of this bone and of the sense of smelling in the Cheiroptera. Cambridge: Harvard University Press.

Apfelbach R, Russ D, Slotnick BM. 1991. Ontogenetic changes in odor sensitivity, olfactory receptor area and olfactory receptor density in the rat. Chem Senses 16:209–218.

Bhatnagar KP, Kallen FC. 1974. Cribriform plate of ethmoid, olfactory bulb and olfactory acuity in forty species of bats. J Morphol 142:71–89.

Buhl H. and Oelschläger HA. 1988. Morphogenesis of the brain in the harbour porpoise. J Comp Neurol 277:109–125.

Colbert MW, Racicot R, Rowe T. 2005. Anatomy of the cranial endocast of the bottlenose dolphin, *Tursiops truncatus*, based on HRXCT. J Mamm Evol 12:195–207.

De Beer SG. 1937. The development of the vertebrate skull. Oxford: Clarendon Press.

Doucette R. 1991. PNS-CNS transitional zone of the first cranial nerve. J Comp Neurol 312:451–466.

Doty RL, Shaman P, Dann M. 1984. Development of the University of Pennsylvania smell identification test: a standardized microencapsulated test of olfactory function. Physiol Behav 32: 489–502.

Estes JA. 1989. Adaptations for aquatic living by carnivores. In: Gittleman JL, editor. Carnivore behavior, ecology, and evolution. Ithaca: Cornell University Press. p 242–282.

Estes RD. 1991. The behavior guide to African mammals: including hoofed mammals, carnivores, primates. Berkeley: University of California Press.

Ewer RF. 1998. The carnivores. Ithaca: Cornell University Press.

Farbman A. 1992. Cell biology of olfaction. Cambridge: Cambridge University Press.

Friedrich RW. 2006. Mechanisms of odor discrimination: neurophysiological and behavioral approaches. Trends Neurosci 29: 40–47.

Garcia N, Santos E, Arsuaga JL, Carretero JM. 2007. Endocranial morphology of the *Ursus deningeri* von Reichenau 1904 from the Sima de Los Huesos (Sierra de Atapuerca) Middle Pleistocene site. J Vert Paleontol 27:1007–1017.

Gittleman JL. 1991. Carnivore olfactory bulb size: allometry, phylogeny, and ecology. J Zool 225:253–272.

Godfrey SJ, Geisler J, Fitzgerald EM. 2013. On the olfactory anatomy in an archaic whale (Protocetidae, Cetacea) and the minke whale *Balaenoptera acutorostrata* (Balaenopteridae, Cetacea). Anat Rec 296:257–272.

Green PA, Valkenburgh B, Pang B, Bird D, Rowe T, Curtis A. 2012. Respiratory and olfactory turbinal size in canid and arctoid carnivorans. J Anat 221:609–621.

Hayden S, Bekaert M, Crider TA, Mariani S, Murphy W, Teeling E. 2010. Ecological adaptation determines functional mammalian olfactory subgenomes. Genome Res 20:1–9.

Hoch E. 2000. Olfaction in whales: evidence from a young odontocete of the Late Oligocene North Sea. Hist Biol 14:67–89.

Jerison HJ. 1973. Evolution of the brain and intelligence. New York: Academic Press.

Joeckel RM, Bond HW, Kabalka GW. 1997. Internal anatomy of the snout and paranasal sinuses of Hyaenodon (Mammalia, Creodonta). J Vert Paleontol 17:440–446.

Kalmey JK, Thewissen JGM, Dluzen DE. 1998. Age-related size reduction of foramina in the cribriform plate. Anat Rec 251:326–329.

Kandel ER, Schwartz JH, Jessell TM. 2000. Principles of neural science. New York: McGraw-Hill.

Kavoi B, Makanya A, Hassanali J, Carlsson HE, Kiama S. 2010. Comparative functional structure of the olfactory mucosa in the domestic dog and sheep. Ann Anat 192:329–337.

Kielan-Jaworowska Z. 2004. Mammals from the age of dinosaurs: origins, evolutions, and structure. New York: Columbia University Press.

Kishida T, Kubota S, Shirayama Y, Fukami H. 2007. The olfactory receptor gene repertoires in the secondary-adapted marine vertebrates: evidence for reduction of the functional proportions in cetaceans. Biol Lett 3:428–430.

Kruuk H. 1972. The spotted hyena: a study of predation and social behavior. Chicago: University of Chicago Press.

Kuhn HJ. 1971. Die Entwicklung und Morphologie des Schädels von *Tachyglossus aculeatus*. Abhandlungen der Senckenbergischen naturforschenden Gesellschaft 528:226.

Maier W. 1993. Cranial morphology of the therian common ancestor, as suggested by the adaptations of neonate marsupials. In: Szalay FS, Novacek MJ, McKenna MC, editors. Mammal phylogeny. New York: Springer Verlag. p 165–181.

Maier W, Heever JD, Durand F. 1996. New therapsid specimens and the origin of the secondary hard and soft palate of mammals. J Zoological Systematics and Evol Res 34:9–19.

Marshall DA, Blumer L, Moulton, DG. 1981. Odor detection curves for n-pentanoic acid in dogs and humans. Chem Senses 6: 445–453.

Meisami E. 1989. A proposed relationship between increases in the number of olfactory receptor neurons, convergence ratio and sensitivity in the developing rat. Devel Brain Res 46: 9–19.

Menco BPM. 1980. Qualitative and quantitative freeze-fractured studies on olfactory and nasal respiratory structures of frog, ox, rat and dog. Cell Tiss Res 207:183–209.

McCotter RE. 1912. The connection of the vomeronasal nerves with the accessory olfactory bulb in the opossum and other mammals. Anat Rec 6:299–318.

Negus SV. 1958. The comparative anatomy and physiology of the nose and paranasal sinuses. Edinburgh: Livingstone.

Niimura Y, Nei M. 2005. Comparative evolutionary analysis of olfactory receptor gene clusters between humans and mice. Gene 346:13–21.

Niimura Y, Nei M. 2007. Extensive gains and losses of olfactory receptor genes in mammalian evolution. PLoS ONE 2:e708.

Nummela S. 1995. Scaling of the mammalian middle ear. Hear Res 85:18–30.

Nummela S, Pihlström H, Puolamäki K, Fortelius M, Hemilä S, Reuter T. 2013. Exploring the mammalian sensory space: cooperations and trade-offs among senses. J Comp Physiol A 199: 1077–1092.

Oelschläger HA. 1989. Early development of the olfactory and terminalis systems in baleen whales. Brain Behav Evol 34:171–183.

Oelschläger HA. 1992. Development of the olfactory and terminalis systems in whales and dolphins. In: Doty RL, Muller-Schwarze D editors. Chemical signals in vertebrates. Vol. 6. New York: Plenum Press. p 141–147.

Oelschläger HA. 2000. Morphological and functional adaptations of the toothed whale head to aquatic life. Hist Biol 14:33–39.

Olender T, Fuchs T, Linhart C, Shamir R, Adams M, Kalush F, Khen M, Lancet D. 2003. The canine olfactory subgenome. Genomics 83:361–372.

Paulli S. 1900. Über die Pneumaticität des Schädels bei den Säugetieren; eine morphologische Studie. Morphol Jahrb 28:147–178.

Pihlström H, Fortelius M, Hemilä S, Forsman R, Reuter T. 2005. Scaling of mammalian ethmoid bones can predict olfactory organ size and performance. Proc Royal Soc B 272:957–962.

Radinsky LB. 1969. Outlines of canid and felid evolution. Ann N Y Acad Sci 167:277–288.

Rowe TB, Eiting TP, Macrini TE, Ketcham, RA, 2005. Organization of the olfactory and respiratory skeleton in the nose of the gray short-tailed opossum *Monodelphis domestica*. J Mamm Evol 12: 303–336.

Saito H, Kubota M, Roberts RW, Chi Q, Matsunami H. 2004. RTP family members induce functional expression of mammalian odorant receptors. Cell 119: 679–691.

Slater GJ, Harmon LJ, Wegmann D, Joyce P, Revell LJ, Alfaro ME, 2012. Fitting models of continuous trait evolution to incompletely sampled comparative data using approximate Bayesian computation. Evolution 66: 752–762.

Smith TD, Bhatnagar KP, Tuladhar P, Burrows AM. 2004. Distribution of olfactory epithelium in the primate nasal cavity: are microsmia and macrosmia valid morphological concepts? Anat Rec 281: 1173–1181.

Smith TD, Rossie J. 2006. Primate olfaction: anatomy and evolution. In: Warrick B, Castle D, Pantelis C, editors. Olfaction and the brain. New York: Cambridge University Press. p 135–166.

Silver I, Kim C, Mollanji R, Johnston M. 2002. Cerebrospinal fluid outflow resistance in sheep: impact of blocking cerebrospinal fluid transport through the cribriform plate. Neuropathol Appl Neurobiol 28:67–74.

Van Valkenburgh B. 1990. Skeletal and dental predictors of body mass in carnivores. In: Damuth J, MacFadden B, editors. Body size in mammalian paleobiology: estimation and biological implication. Cambridge: Cambridge University Press.

Van Valkenburgh B, Theodor J, Friscia, A, Rowe T. 2004. Respiratory turbinates of canids and felids: a quantitative comparison. J Zool 264:281–293.

Van Valkenburgh B, Curtis A, Samuels JX, Bird D, Fulkerson B, Meachen-Samuels J, Slater GJ. 2011. Aquatic adaptations in the nose of carnivorans: evidence from the turbinates. J Anat 218: 298–310.

Wall WP. 1980. Cranial evidence for a proboscis in Cadurcodon and a review of snout structure in the family Amynodontidae (Perissodactyla, Rhinocerotoidea). J Paleontol 54:968–977.

Wilson DE, Mittermeier RA. 2009. Handbook of the mammals of the world. Vol. 1. Barcelona: Lynx.

Zeller U. 1988. The lamina cribrosa of *Ornithorynchus* (Monotremata, Mammalia). Anat Embryol 178:513–519.